Experimental determination of nitrogen isotope fractionation associated with NH_3 degassing at 0-70 ºC

by

Yuying Deng

A thesis submitted in partial fulfillment of the requirements for the degree of

Master of Science

Department of Earth and Atmospheric Sciences
University of Alberta

Abstract

Ammonia degassing is a common process in natural alkaline water systems (e.g., hydrothermal vents). Nitrogen isotope fractionation factor is an important parameter to quantitatively assess the nitrogen cycle in these systems, but still not constrained yet. In this study, we carried out laboratory experiments to examine the nitrogen isotope behavior during partial degassing of ammonia from an ammonium sulfate solution. The experiments started with ammonium sulfate solution with excess sodium hydroxide. The reaction can be described as: $NH_4^+ + OH^-$ (excess) $\rightarrow NH_3 \bullet nH_2O \rightarrow NH_{3\,(g)} \uparrow$. Nitrogen isotopic ratios were analyzed on remaining ammonium. Two sets of experiments, one under static conditions and the other with N_2 gas bubbling, were carried out at 2, 21, 50, and 70 ºC. The results indicate that the data from the bubbling experiments fit well with a Rayleigh distillation model, suggest that a kinetic isotope fractionation occurred during partial degassing of ammonia. Modeling results gave a fractionation factor of 0.9898 at 2 °C, 0.9918 at room temperature (~21 °C), 0.9935 at 50 °C and 0.9948 at 70 °C. These isotope fractionation factors increase with temperature. A linear fitting yields a relationship between nitrogen isotope fractionation factor and temperature as $10^3 ln\alpha_{NH3 (g)-NH3 (aq)} = 14.6 - 6.8 \cdot \frac{1000}{T}$. On the other hand, nitrogen isotopic data from experiments under static conditions do not fit either equilibrium isotope fractionation (the batch model) or kinetic isotope fractionation (the Rayleigh distillation model). One possible cause is the back dissolution of the degassed ammonia, which is likely associated with another unconstrained isotopic effect. These experimental results provide important insights into the understanding of the alkaline system in the field.

Preface

In this study, I was responsible for carrying out degassing experiments (from experimental design, purchase of necessary parts, experiment processing), sample preparation, and isotope analysis and modeling in this study.

Acknowledgement

Foremost, I wish to express my sincere gratitude to my supervisor Dr. Long Li for his encouragement and inspiration; for his vast knowledge and skill; for his generous help and valuable guidance. I am also grateful to my other two examining committee members Dr. Karlis Muehlenbachs and Dr. Guillermo Hernandez Ramirez for their insightful comments.

Secondly, I would like to thank my colleague Yingzhou Li at University of Alberta for providing his help for this research.

Thirdly, I am grateful to the members of the stable isotopes group: Zhe Zhang, Kan Li. They have given valuable comments and discussions.

Finally, I would also like to say thank you to my parents for their support and encouragement through the past two years.

Table of Content

List of Figures

1. Introduction

Nitrogen cycle involves several major nitrogen species at various valence states, e.g., nitrate, nitrite, dinitrogen, ammonium/ammonia. Among these valence states, ammonium/ammonia is the most reduced form and the key species linking the biological nitrogen cycle on Earth's surface and the geological nitrogen cycle from Earth's surface to the interior and back to surface. This is because ammonium/ammonia can be involved as either reactant or product in a variety of biological processes, such as nitrification (e.g., Luther et al., 1997), denitrification (e.g., Sigman et al., 2003), and anammox (e.g., Kuypers et al., 2003), and in a variety of geological processes, such as abiotic nitrogen reduction (Li et al., 2014), nitrogen remobilization during hydrothermal alteration (Bebout et al., 1999; Busigny et al., 2005; Li et al., 2007), metamorphic devolatilization (Mingram and Bräuer, 2001; Jia, 2006), redox-controlled nitrogen transformation from the crust to the mantle (Mikhail and Sverjensky, 2014). Thus, the geochemical behavior of ammonium/ammonia in natural environments is a crucial parameter to interpret the geological record and understand the nitrogen cycle.

In aqueous medium (including ground water and hydrothermal fluid) that harbors biological and geological nitrogen recycling, the relative proportion of ammonium or ammonia is strongly dependent on water pH (Li et al., 2012; Mikhail et al., 2017). In alkaline solution, ammonium can be dissociated into ammonia. In open systems, such as alkaline lakes, hot springs, and hydrothermal vents (see Li et al., 2012 for discussion), ammonia can easily degas out of the system. Strong ammonia degassing is also common in agricultural land where ammonium/ammonia content is high (Meisinger and Jokela, 2000). Ammonia degassing has strong impacts on ecosystems in these environments and may affect other environments through

transportation and reprecipitation of the volatilized ammonia. To constrain the effect of ammonia degassing, it requires an efficient geochemical tool.

One of the unique geochemical signatures observed in the alkaline water systems is the significant ^{15}N enrichment in the dissolved ammonium. For example, Talbot and Johannessen (1992) reported high δ^{15}N values of up to 18‰ in Lake Bosumtwi, Ghana, West Africa, which is a modern alkaline lake with pH values around 9.1-9.6. Lent et al. (1995) reported high δ^{15}N values of 8.5‰ to 28.0‰ for organic matter from Devils Lake, North Dakota with a pH value of around 8.8 (Fritz, 1990). Collister et al. (1992) also observed high δ^{15}N values from 10.8‰ to 20.7‰ for organic matters in the Eocene Green River Formation in the western USA. These observations suggest that considerable isotopic effects may occur during ammonia degassing. An isotopic effect associated with ammonia degassing is also supported by the observation from the hot springs in Yellow Stone National Park. Holloway et al. (2011) found that, compared with the source, ammonium in high-pH waters in Yellow Stone National Park was enriched in ^{15}N whereas ammonium in low-pH waters is isotopically unfractionated. Furthermore, extreme ^{15}N enrichment in organic matter with δ^{15}N values up to 50‰ has been observed in the 2.72 Ga lacustrine Tumbiana Formation of the Fortescue Group in Western Australia (Thomazo et al., 2011; Stüeken et al., 2015). Combined with lithological and geochemical characteristics, Stüeken et al. (2015) interpreted these extremely high δ^{15}N values to result from a large ancient alkaline lake in 2.72 Ga.

To better assess these hypotheses and to quantitatively model the ammonia degassing-related nitrogen cycle, it is crucial to determine the nitrogen isotope fractionation during these processes. Some previous studies have provided the nitrogen isotope fractionation factor between ammonium and ammonia using theoretical thermodynamic equilibration models (Urey, 1947;

Scalan, 1959; Hanschmann, 1981; Petts et al., 2015). However, these fractionation factors can hardly explain the field data from low-temperature environments. In a recent experimental study, Li et al. (2012) found that the ammonium/ammonia behavior in alkaline conditions could be more complicated than previously thought and proposed a two-step process: ammonium dissociation into aqueous ammonia (Equation 1) followed by ammonia degassing from aqueous ammonia (Equation 2):

$$NH_4^+{}_{(aq)} + OH^- \rightleftharpoons NH_3 \bullet H_2O_{(aq)} \tag{1}$$

$$NH_3 \bullet H_2O_{(aq)} \rightarrow NH_{3\,(g)} \uparrow + H_2O \tag{2}$$
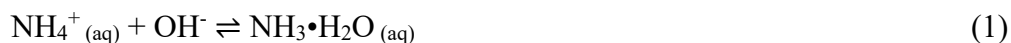
Based on careful experimental control on partial dissociation of ammonium and complete degassing of produced ammonia, Li et al. (2012) determined the nitrogen isotope fractionation factors in the first step reaction, which shows large equilibrium isotope fractionations between ammonium and ammonia for ~45‰ at 23ºC and ~34‰ at 70 ºC. However, the isotope fractionation factor for ammonia degassing from aqueous ammonia is still not constrained yet. To fill this gap, we carried out laboratory experiments to determine the nitrogen isotope fractionation associated with ammonia degassing between 0ºC and 70 °C, a temperature range covering most of the aqueous systems on Earth's surface.

2. Experimental setup

2.1. Chemicals used for experiments

The chemicals used in the experiments include a 0.2 M ammonium sulfate solution, which was prepared by dissolving commercial ammonium sulfate solids (measured $\delta^{15}N$ = 0.07‰; Li et al., 2012) into distilled water, 12.5 M sodium hydroxide solution (NaOH), and 8 M sulfuric acid (H_2SO_4).

2.2. Ammonia degassing experiments

Experiments were carried out in a fume hood at 2 °C, room temperature, 50 and 70 °C. All these temperatures were direct measurements on the ammonium sulfate solution rather than air or water bath temperatures. The solution temperature under room temperature over the course of our experiments was 21 ± 2 °C. Experiments at temperatures higher than room temperature were controlled in a heating water bath, which gave an error of ± 1 °C. Experiments at temperatures lower than room temperature were also controlled in a water bath filled with ice-water mixture. The real temperature measurements on the ammonium sulfate solution were 2 ± 1 °C over the course of experiments.

Experiments at all temperatures were carried out without (Figure 1) and with (Figure 2) bubbling of N_2. The sets of experiments without bubbling of N_2 are hereafter referred as "static experiments" and the sets of experiments with bubbling of N_2 are hereafter referred as "bubbling experiments".
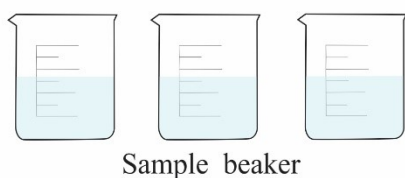
a Experiments at room temperature (21°C)   **b** Experiments at 2°C, 50°C, 70°C
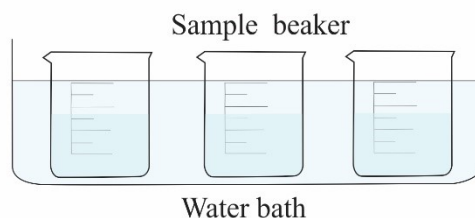
Figure 1. Schematic diagrams illustrating experimental setup for ammonia degassing under static conditions: (a) at room temperature (~21 °C); (b) at 2 °C, 50 °C, and 70 °C.

For each experiment, 50 ml ammonium sulfate solution measured by a volumetric flask was transferred to a beaker. For bubbling experiments, N_2 was introduced into the solution and started to bubble immediately. After the ammonium sulfate solution equilibrated with ambient temperature, 5 ml 12.5 M NaOH was added into the solution, which was disturbed by a glass rod quickly to homogenize the NaOH in the solution. Because of the added OH^- is stoichiometrically more than 3 times of the NH_4^+ in the solution, the excess hydroxide ensures complete transformation of ammonium to aqueous ammonia. After a certain period of ammonia degassing, the remaining ammonia in the solution(pH>13) was fixed by adding 8M H_2SO_4 to acidify the solution to pH of 3-5, a range that can practically best balance between ammonium preservation and sample drying (Li et al., 2012). The remaining solution after degassing was then transferred to a volumetric flask and adjusted back to 50 ml. Two milliliters of solution was taken from the 50 ml solution by a pipette and transferred to a pre-weighed small beaker, dried in an oven at 80 °C then weighed again to quantify the solids.

a Experiments at room temperature (21°C)   **b** Experiments at 2°C, 50°C, 70°C

N_2 Tank

N_2 Tank

Water bath
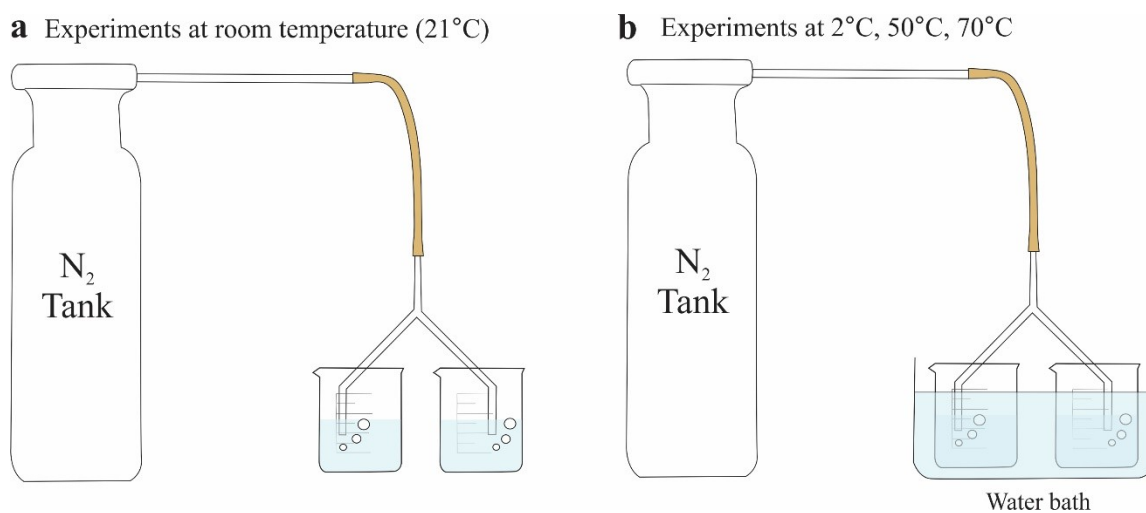
Figure 2. Schematic diagrams showing experimental setup for ammonia degassing with dinitrogen gas bubbling.

2.3. Analytical techniques

The experimental samples were quantified and measured for nitrogen isotope compositions using an elemental analyzer (EA) coupled with an isotope ratio mass spectrometer (IRMS) at the University of Alberta.

Dried solid material (a mixture of ammonium sulfate and sodium sulfate) after the ammonia degassing experiment was crushed into fine powder, from which an aliquot was weighed and wrapped together with a small quantity of vanadium oxide into a tin capsule. The capsule was then loaded and combusted in an EA (model: Flash 2000) at 1000 ºC. The produced N_2 was carried by a high-purity helium stream to an IRMS (model: Delta V Plus) for isotopic measurement.

Nitrogen yield was calculated by the intensity of the nitrogen peak on the IRMS based on a calibrated relationship between peak intensity and weight of the ammonium sulfate standards (Figure 3). The nitrogen yield was then integrated with the weight of the solid mixture wrapped into the tin capsule to calculate the concentration of the remaining ammonia after the ammonia degassing experiment.

Three standards including two international standards (IAEA-N-1 and IAEA-N-2) and one lab standard, all in form of ammonium sulfate, were measured in parallel to samples. IAEA-N-1 and IAEA-N-2 were used to calibrate the isotopic ratios of samples and the lab standard, which gave a 2σ standard deviation better than 0.3‰.
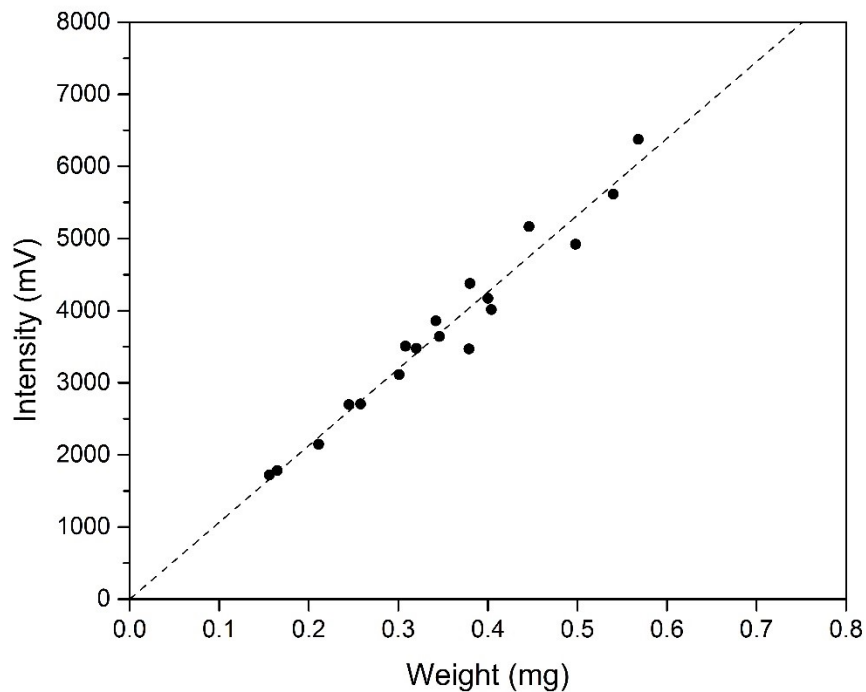
Figure 3. Relationship between sample weight (mg) of pure ammonium sulfate standard and mass 28 signal intensity (mV).

3. Results

All the experimental data were listed in Table 1.

Overall, ammonia degassing occurred very fast in our degassing conditions. A complete removal of ammonia was reached within 4 hours at 2 ℃, 2.25 hours at 21 ℃, 1 hours at 50 ℃, and 20 minutes at 70 ℃ under static condition. Although the extents of ammonia degassing in both static and bubbling experiments do not appear to follow strictly with degassing time, it is clear that the bubbling experiments showed more extents of ammonia degassing than the static experiments at the same temperature and degassing time.

With the progress of ammonia degassing, the remaining ammonia in both static and bubbling experiments became more enriched in ^{15}N (Figure 4), with larger magnitudes in the bubbling experiments (Figure 4).
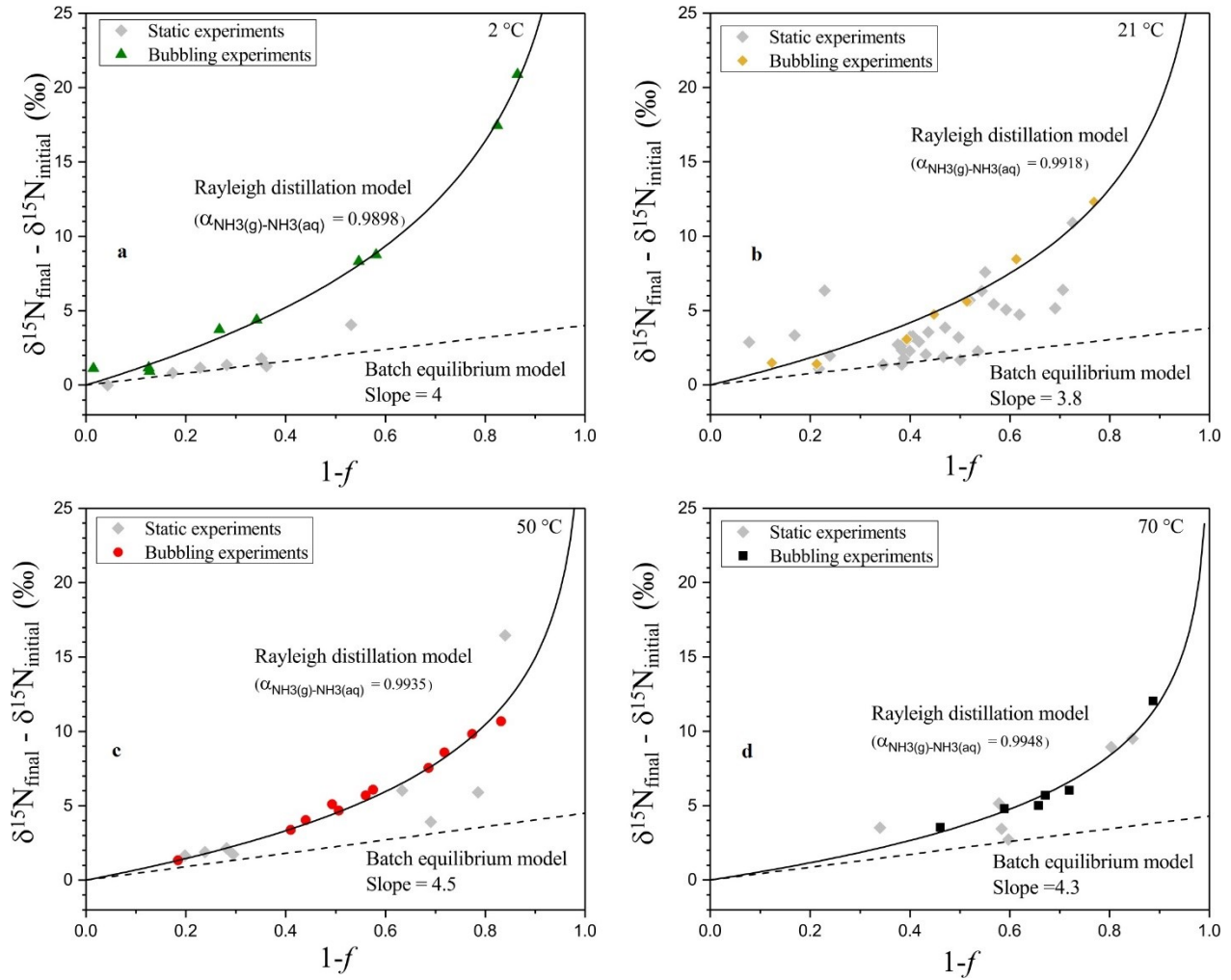
Figure 4. Evolution of the $\delta^{15}N$ values of the remaining $NH_{3(aq)}$ with theoretical batch and Rayleigh modeling of fractionation factor at 2 ℃ (a), 21 ℃ (b), 50 ℃ (c) and 70 ℃ (d). Fractionation factor for Rayleigh model was calculated by data from bubbling experiments. Fractionation factor for batch model was estimated from the lower boundary of static experiments.

4. Discussion

4.1 Nitrogen isotope fractionations associated with ammonia degassing

It is clearly shown in Figure 4 that the data from the bubbling experiments display a good non-linear increasing trend in the $\delta^{15}N$ of remaining ammonia with the progress of ammonia degassing. This trend resembles the isotopic result of a kinetic isotopic effect, which can be described by the Rayleigh distillation model (Mariotti et al., 1981)

$$\varepsilon_{P/S}=10^{3\cdot}\ln[(1+10^{-3}\delta_S)/(1+10^{-3}\delta_{S,0})]/\ln f \qquad (3)$$

in which ε is the isotope enrichment factor between the product (in this case, degassed ammonia) and substrate (in this case, aqueous ammonia), f is the fraction of the remaining ammonia, $\delta_{S,0}$ and δ_S are the $\delta^{15}N$ values of the initial and remaining ammonia.

On the $10^3\ln[(1+10^{-3}\delta_S)/(1+10^{-3}\delta_{S,0})]$ vs. lnf diagram (Figure 5), the data from the bubbling experiments at all temperatures display good linear relationship. Linear fitting of the data yielded ε values (i.e., the slope of the fitted line) as -10.2‰ at 2 ºC, -8.2‰ at 21 ºC, -6.5‰ at 50 ºC, and -5.2‰ at 70 ºC. These can be alternatively expressed in term of kinetic nitrogen isotope fractionation factor between degassed ammonia and the remaining ammonia in solution (i.e., $\alpha_{NH3-NH3\cdot H2O} = 1 + 10^{-3} \varepsilon_{NH3-NH3\cdot H2O}$) as 0.9898 at 2 °C, 0.9918 at 21 ºC, 0.9935 at 50 °C, and 0.9948 at 70 °C.

The rate-determined kinetic isotope fractionation factor for nitrogen isotope can be described in term of temperature as (Li et al., 2009):

$$\alpha \propto \frac{R_{N-15}}{R_{N-14}} = \frac{e^{-E_{a1}/kT}}{e^{-E_{a2}/kT}} = e^{-E_a/kT} \qquad (4)$$

where R is the rate of the chemical reaction, E_a is the activation energy (in J mol^{-1}), T is temperature (Kelvin).

Rearrange equation 4,

$$\ln \alpha \propto -A/T \qquad (5)$$

where $A = E_a/k$.
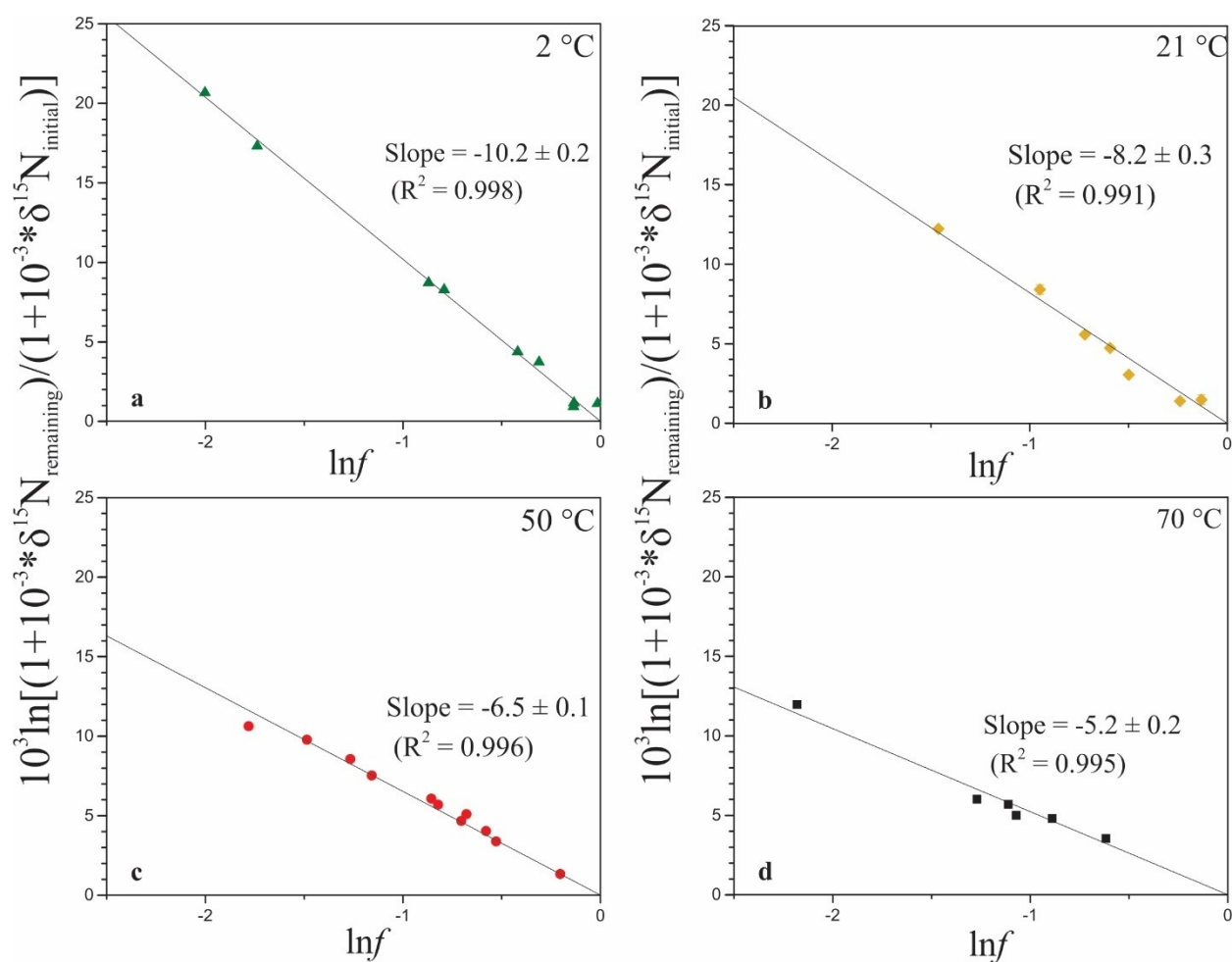
Figure 5. Modeling of nitrogen isotope fractionation factor between aqueous ammonia and gaseous ammonia through bubbling experiments at 2 ºC (a), 21 ºC (b), 50 ºC (c) and 70 ºC (d).

According to Equation 5, the isotope fractionation factors are expected to decrease with increasing temperatures. In the experimental temperature range of 2 to 70 °C, we do observe a linear relationship between the nitrogen isotope fractionation factors and ammonia degassing temperature (Figure 6) as:

$$10^3 \ln\alpha_{NH3\ (g)\text{-}NH3\ (aq)} = 14.6 - 6.8 \cdot \frac{1000}{T} \qquad (6)$$

in which T is temperature in Kelvin.
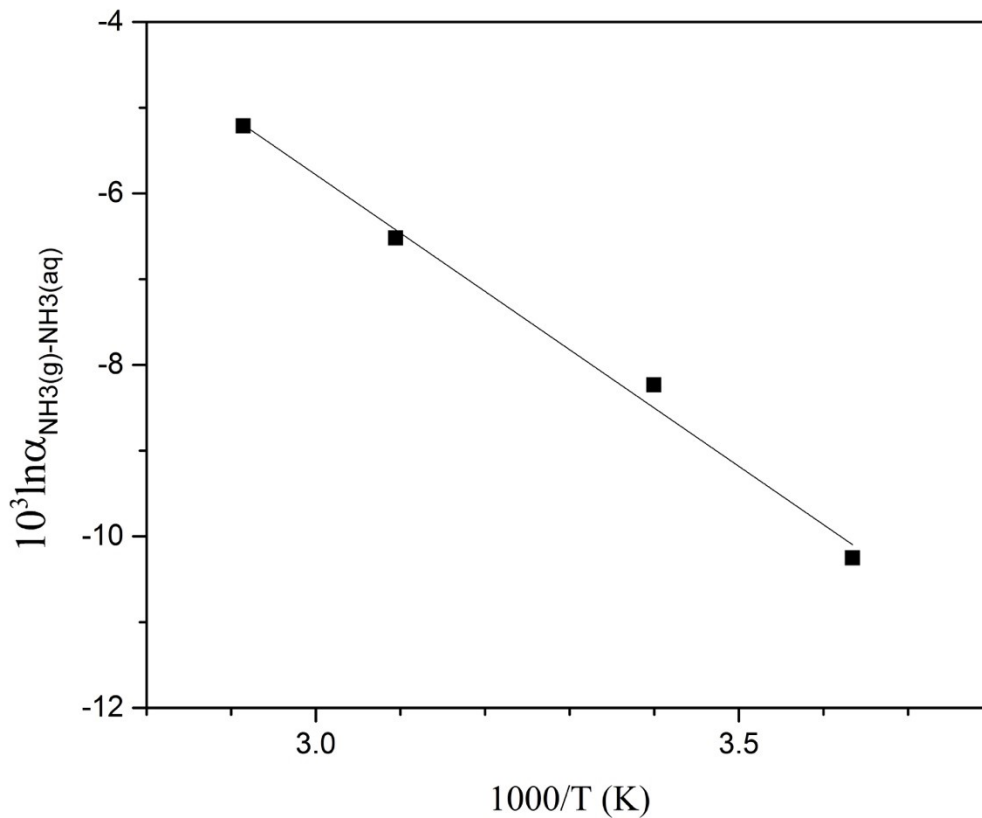
Figure 6. Relationship between $\alpha_{NH3\ (g)\text{-}NH3\ (aq)}$ and temperature.

4.2 Ammonium degassing process under static condition

While the nitrogen isotope compositions of the remaining ammonia in solutions from the bubbling experiments follow the Rayleigh distillation model (i.e., a kinetic isotopic effect), the nitrogen isotope compositions of the remaining ammonia from the static experiments show more complicated features (Figure 4): (1) the magnitudes of ^{15}N enrichment in the remaining ammonia of the static experiments are smaller than those of bubbling experiments, (2) the magnitudes of ^{15}N enrichment in the remaining ammonia of the static experiments are irreproducible, which results in scattered data distribution below the upper curve defined by the bubbling experiments on Figure 4, and (3) the results of the static experiments cannot be modeled by either Rayleigh distillation model or the batch distillation model. We speculate that the deviation of the static experimental data from the kinetic effect defined by the bubbling experimental data may be attributed to back dissolution of part of the degassed ammonia.

Following the re-dissolution of ammonia in the ammonium solution, the isotope exchange between ammonia gas and aqueous ammonia becomes two ways, which can be described as:

$$NH_{3\ (gas)} + H_2O \rightleftharpoons NH_3 \bullet n\ H_2O\ _{(aq)} \tag{7}$$

Ideally, this reverse reaction may result in an equilibrium isotope fractionation between gaseous ammonia and aqueous ammonia. Accordingly, we can interpret the diminished ^{15}N enrichments in the remaining ammonia in the static experiments as isotopic exchange toward equilibrium isotope fractionation. If we assume that the lower data boundary of the static experiments is close to equilibrium isotope fractionation, we can use a

batch model to determine the equilibrium isotope fractionation factors between the gaseous

ammonia and aqueous ammonia. The batch model can be described as (Valley, 1986):

$$10^3 \cdot \ln\alpha_{\text{NH3 (g)-NH3 (aq)}} = -\frac{\delta15N_{Final} - \delta15N_{Initial}}{1 - f} \qquad (8)$$

The isotopic change of the remaining ammonia in a batch model was marked by the dashed

linear lines on Figure 4. The modeling gave equilibrium isotope fractionation factors between

gaseous ammonia and aqueous ammonia of ~ -4.0‰ at 2 °C, ~ -3.8‰ at 21 °C, ~ -4.5‰ for

50 °C and ~ -4.3°C for 70 °C. These data do not show a strict temperature-dependent

relationship, which is in fact expected for equilibrium isotope fractionation, and thus are not

accurate. This may be attributed to a relatively small dataset of our static experiments.

Kirshenbaum et al. (1947) suggested an equilibrium isotope fractionation factor of ~ -5‰

between $NH_{3(g)}$ and $NH_{3(aq)}$ at 25°C. Some recent theoretical calculations gave equilibrium

nitrogen isotope fractionations between gaseous and aqueous ammonia for about 5.1‰ at 0 °C

and 3.1‰ at 70 ºC (Zhang, personal communication). Our first order estimates surprisingly fit

well in this range. This proves our speculation.

4.3 Implication to the interpretation of field data

(1) Various isotope effects in natural environments

Our experiments have demonstrated that the isotopic effect associated with ammonia

degassing may vary from kinetic isotope fractionation to equilibrium isotope fractionation. Thus,

great cautions should be taken to choose isotope fractionation factors for different geological

conditions. For example, in a closed or semi-closed system, equilibrium isotope fractionation

may be reached between ammonia and aqueous ammonia. This may apply to the long isolated

deep fracture water system because such system is mostly stable during the isolation and thus regarded as (semi-) closed system. In contrast, the marine hydrothermal vents and hot springs are regarded as open systems, which commonly contain other gases, such as N_2, CO_2, or CH_4, and thus may provide a condition similar to our bubbling experiments. As a result, ammonia degassed from hydrothermal vents and hot springs could be dominated by the kinetic isotopic effect.

(2) Constraints on the nitrogen cycle in the atmosphere

Xiao et al. (2015) analysed the $\delta^{15}N$ values of rainwater in Guiyang, China, between 2009 to 2010. The results show a Rayleigh distillation-like pattern. Xiao et al. (2015) attributed this pattern to nitrogen isotope fractionation between NH_4^+-$NH_{3(aq)}$ and $NH_{3(aq)}$-$NH_{3(g)}$, where isotope enrichment factors for $NH_{3(aq)}$-$NH_{3\ (g)}$ applied in Xiao et al. (2015) is 10.4 ± 4.3‰. Our experimental study demonstrates the validity of this value and proves that the degassing model can apply to explain the atmospheric nitrogen isotope data.

(3) Insights into the 2.7 Ga alkaline lake environments from $\delta^{15}N$ of the Tumbiana Formation

The Tumbiana Formation has the highest $\delta^{15}N$ values (from 22.9‰ to 44.0‰) in the geological record (Thomazo et al., 2011; Stüeken et al., 2015). Stüeken et al. (2015) interpreted these data to mainly reflect the isotope effect of dissociation of ammonium to ammonia (Li et al., 2012). These authors further pointed out that, because the highest $\delta^{15}N$ value of up to 50‰ cannot be accounted by the isotope fractionation factors in Li et al. (2012), additional kinetic isotope effect likely associated with ammonia degassing should be considered. However, although there is a strong kinetic isotopic effect associated with ammonia degassing, the experiments in this study and those in Li et al. (2012) also show that ammonia degassing occurs

very fast and efficient ammonia removal can be easily achieved. In addition, the experiments by Li et al. (2012) further revealed that the nitrogen isotope exchange between aqueous ammonia and remaining ammonium is slow enough and can be ignored during the ammonia degassing from aqueous ammonia. Therefore, the kinetic isotopic effect associated with ammonia degassing is difficult to be transferred into the remaining ammonium and should be lost with the complete removal of ammonia from the water. We think the high δ^{15}N values in the Tumbiana Formation do rely on the isotopic effect of ammonium dissociation. Most of the Tumbiana data fall below 40‰, except one data up to 50‰, which can be explained either by a larger isotope fractionation at lower temperatures (Figure 7) or diagenetic effect that can cause ^{15}N enrichment in remaining organic matter. We propose that the strongly variable δ^{15}N values in the Tumbiana Formation reflect strong fluctuation of the alkalinity of the lake water over time, which could be caused by variable inputs of alkaline hydrothermal fluids. When hydrothermal input brought a relatively small quantity of hydroxide, expressed as small $[OH^-]/[NH_4^+]$ ratio, the extent of ammonium loss would be small, resulting in relatively low δ^{15}N value of the remaining ammonium (Figure 7). When hydrothermal input brought a large quantity of hydroxide, i.e., $[OH^-]/[NH_4^+]$ ratio moves toward to 1, the extent of ammonium loss would be large, resulting in very high δ^{15}N value of the remaining ammonium (Figure 7).
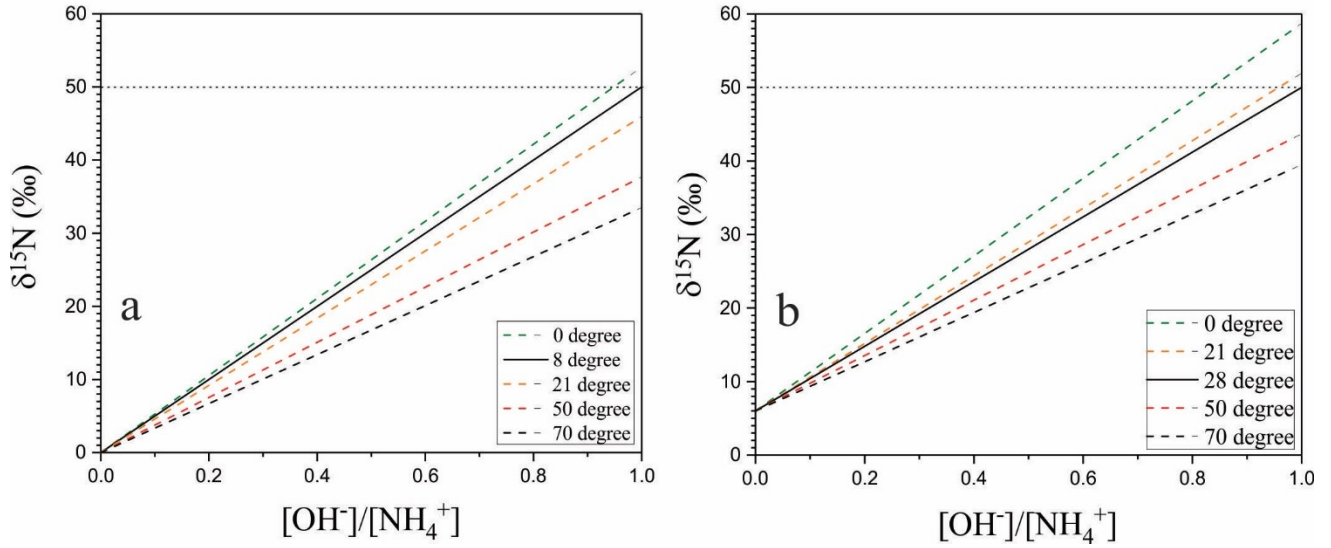
Figure 7. $\delta^{15}N$ value of remaining ammonium after partial ammonium dissociation caused by input of various quantity of hydroxide (expressed as [OH$^-$]/[NH$_4^+$] ratio) from a hydrothermal source. Different lines represent different temperatures, based on relationship between nitrogen equilibrium isotope fractionation and temperature: $10^3 \ln\alpha_{NH4+-NH3\ (aq)} = 25.94 \cdot \frac{1000}{T} - 42.25$ (Li et al., 2012). Assuming a starting $\delta^{15}N$ value: (a) initial $\delta^{15}N$ value is 0‰; (b) initial $\delta^{15}N$ value is 6‰.

5. Conclusion

1. Our experimental investigations reveal that fast ammonia degassing can cause a kinetic nitrogen isotopic effect. The nitrogen fractionation factors between gaseous ammonia and aqueous ammonia are 0.9898 at 2 °C, 0.9918 at 21 °C, 0.9935 at 50 °C and 0.9948 at 70 °C. These fractionation factors show a good linear relationship with temperature. Linear fitting between the nitrogen isotope fractionation factor and temperature (Kelvin) yielded a relationship as $10^3 \ln\alpha_{NH3\ (g)-NH3\ (aq)} = 14.6 - 6.8 \cdot \frac{1000}{T}$.

16

2. Our experimental investigations also indicate that, when the removal of degassed ammonia is not efficient, ammonia may dissolve back to the fluid. A different isotopic effect is observed during this process, which can result in a shift of the $\delta^{15}N$ values of the remaining ammonia in the fluid toward the equilibrium isotope fractionation.

6. Future work

First, more experiments are required to better define the lower boundary of static experiments (Figure 4). In this study, the batch model was applied to interpret the lower boundary defined by the experimental data of static experiments. However, the fractionation factors obtained from batch model (i.e., slope of the lower boundary) did not present a temperature-dependent relationship, which is expected for equilibrium isotope fractionation. To better constrain the lower boundary, it requires more experimental studies in a semi-closed to a closed system, where the gaseous ammonia could possibly have sufficient isotope exchange with aqueous ammonia instead of being instantly removed from the system by dinitrogen gas bubbling. Another way to look into this problem may carry out experiments by dissolving the gaseous ammonia into solution to determine the nitrogen isotope fractionation factors for the $NH_{3\ (g)}$-$NH_{3\ (aq)}$ system.

Second, more experimental work at higher temperatures would be necessary. The experiments in this study yielded an excellent relationship between temperature and nitrogen isotope fractionation factors for the gaseous and aqueous ammonia pair, but only limited in a small temperature range from 0-70 °C. However, natural hot springs and hydrothermal systems can have temperatures as high as 200-300 °C. Although an extrapolation of the relationship

17

defined in this study may provide a reference for the isotope fractionation factors at higher temperatures, it is uncertain how valid the extrapolation can work. More experimental study at higher temperatures for the gaseous and ammonium system to 300 °C would be necessary to fill this gap.

7. References

Bebout, G.E., Ryan, J.G., Leeman, W.P. and Bebout, A.E. (1999) Fractionation of trace elements by subduction-zone metamorphism—effect of convergent-margin thermal evolution. Earth and Planetary Science Letters 171, 63-81.

Busigny, V., Ader, M. and Cartigny, P. (2005) Quantification and isotopic analysis of nitrogen in rocks at the ppm level using sealed tube combustion technique: A prelude to the study of altered oceanic crust. Chemical geology 223, 249-258.

Collister, J.W., Summons, R.E., Lichtfouse, E. and Hayes, J.M. (1992) An isotopic biogeochemical study of the Green River oil shale. Organic Geochemistry 19, 265-276.

Fritz, S.C. (1990) Twentieth-century salinity and water-level fluctuations in Devils Lake, North Dakota: Test of a diatom-based transfer function. Limnology and Oceanography 35, 1771-1781.

Hanschmann, G. (1981) Berechnung von Isotopieeffekten auf quantenchemischer Grundlage am Beispiel stick-stoffhaltiger Moleküle. ZfI-Mitteilungen 41, 19-39.

Holloway, J.M., Nordstrom, D.K., Böhlke, J., McCleskey, R.B. and Ball, J.W. (2011) Ammonium in thermal waters of Yellowstone National Park: processes affecting speciation and isotope fractionation. Geochimica et Cosmochimica Acta 75, 4611-4636.

Jia, Y. (2006) Nitrogen isotope fractionations during progressive metamorphism: A case study from the Paleozoic Cooma metasedimentary complex, southeastern Australia. Geochimica et cosmochimica acta 70, 5201-5214.

Kirshenbaum, I., Smith, J.S., Crowell, T., Graff, J. and McKee, R. (1947) Separation of the nitrogen isotopes by the exchange reaction between ammonia and solutions of ammonium nitrate. The Journal of Chemical Physics 15, 440-446.

Kuypers, M.M., Sliekers, A.O., Lavik, G. and Schmid, M. (2003) Anaerobic ammonium oxidation by anammox bacteria in the Black Sea. Nature 422, 608.

Lent, R.M., Lyons, W.B., Showers, W.J. and Johannesson, K.H. (1995) Late holocene paleoclimatic and paleobiologic records from sediments of Devils Lake, North Dakota. Journal of Paleolimnology 13, 193-207.

Li, L., Bebout, G.E. and Idleman, B.D. (2007) Nitrogen concentration and δ 15 N of altered oceanic crust obtained on ODP Legs 129 and 185: insights into alteration-related nitrogen enrichment and the nitrogen subduction budget. Geochimica et Cosmochimica Acta 71, 2344-2360.

Li, L., Cartigny, P. and Ader, M. (2009) Kinetic nitrogen isotope fractionation associated with thermal decomposition of NH 3: Experimental results and potential applications to trace the origin of N 2 in natural gas and hydrothermal systems. Geochimica et Cosmochimica Acta 73, 6282-6297.

Li, L., Lollar, B.S., Li, H., Wortmann, U.G. and Lacrampe-Couloume, G. (2012) Ammonium stability and nitrogen isotope fractionations for–NH 3 (aq)–NH 3 (gas) systems at 20–70° C and pH of 2–13: Applications to habitability and nitrogen cycling in low-temperature hydrothermal systems. Geochimica et Cosmochimica Acta 84, 280-296.

Li, L., Zheng, Y.-F., Cartigny, P. and Li, J. (2014) Anomalous nitrogen isotopes in ultrahigh-pressure metamorphic rocks from the Sulu orogenic belt: Effect of abiotic nitrogen reduction during fluid–rock interaction. Earth and Planetary Science Letters 403, 67-78.

Luther, G.W., Sundby, B., Lewis, B.L., Brendel, P.J. and Silverberg, N. (1997) Interactions of manganese with the nitrogen cycle: alternative pathways to dinitrogen. Geochimica et Cosmochimica Acta 61, 4043-4052.

Mariotti, A., Germon, J., Hubert, P., Kaiser, P., Letolle, R., Tardieux, A. and Tardieux, P. (1981) Experimental determination of nitrogen kinetic isotope fractionation: some principles; illustration for the denitrification and nitrification processes. Plant and soil 62, 413-430.

Meisinger, J. and Jokela, W. (2000) Ammonia volatilization from dairy and poultry manure. Managing nutrients and pathogens from animal agriculture. NRAES-130. Natural Resource, Agriculture, and Engineering Service, Ithaca, NY, 334-354.

Mikhail, S., Barry, P.H. and Sverjensky, D.A. (2017) The relationship between mantle pH and the deep nitrogen cycle. Geochimica et Cosmochimica Acta 209, 149-160.

Mikhail, S. and Sverjensky, D.A. (2014) Nitrogen speciation in upper mantle fluids and the origin of Earth's nitrogen-rich atmosphere. Nature Geoscience 7, 816.

Mingram, B. and Bräuer, K. (2001) Ammonium concentration and nitrogen isotope composition in metasedimentary rocks from different tectonometamorphic units of the European Variscan Belt. Geochimica et Cosmochimica Acta 65, 273-287.

Petts, D., Chacko, T., Stachel, T., Stern, R. and Heaman, L. (2015) A nitrogen isotope fractionation factor between diamond and its parental fluid derived from detailed SIMS analysis of a gem diamond and theoretical calculations. Chemical Geology 410, 188-200.

Scalan, R.S. (1959) The isotopic composition, concentration, and chemical state of the nitrogen in igneous rocks. University of Arkansas, Fayetteville.

Sigman, D., Robinson, R., Knapp, A., Van Geen, A., McCorkle, D., Brandes, J. and Thunell, R. (2003) Distinguishing between water column and sedimentary denitrification in the Santa Barbara Basin using the stable isotopes of nitrate. Geochemistry, Geophysics, Geosystems 4.

Stüeken, E.E., Buick, R. and Schauer, A.J. (2015) Nitrogen isotope evidence for alkaline lakes on late Archean continents. Earth and Planetary Science Letters 411, 1-10.

Talbot, M.R. and Johannessen, T. (1992) A high resolution palaeoclimatic record for the last 27,500 years in tropical West Africa from the carbon and nitrogen isotopic composition of lacustrine organic matter. Earth and Planetary Science Letters 110, 23-37.

Thomazo, C., Ader, M. and Philippot, P. (2011) Extreme 15N-enrichments in 2.72-Gyr-old sediments: evidence for a turning point in the nitrogen cycle. Geobiology 9, 107-120.

Urey, H.C. (1947) The thermodynamic properties of isotopic substances. Journal of the Chemical Society (Resumed), 562-581.

Valley, J.W. (1986) Stable isotope geochemistry of metamorphic rocks. Stable Isotopes in High Temperature Geological Processes, 445-489.

Xiao, H.-W., Xiao, H.-Y., Long, A.-M. and Liu, C.-Q. (2015) δ 15 N–NH 4+ variations of rainwater: Application of the Rayleigh model. Atmospheric Research 157, 49-55.

8. Appendix

Table 1. Results of degassing experiments at 2 °C to 70 °C.

Treatment	Experimental duration	Remaining NH$_4$ concentration (μM)	f$_{Remaining}$	$\delta^{15}N_{Remaining}$ (‰)	$\delta^{15}N_{Remaining}$ - $\delta^{15}N_{Initial\ NH4+}$ (‰)
initial solution		400000			
2°C experiments					
static					
	15 mins	661.26	0.83	0.08	0.81
	30 mins	765.25	0.96	1.04	-0.01
	1 hr	617.1	0.77	-0.32	1.16
	1.5 hrs	518.72	0.65	-1.08	1.8
	2 hrs	574.37	0.72	-0.56	1.35
	3 hrs	510.45	0.64	-0.56	1.26
	4 hrs	374.98	0.47	-3.52	4.06
N$_2$ bubbling					
	5 mins	788.1	0.99	1.19	1.12
	15 mins	697.87	0.87	0.99	0.92
	30 mins	699.24	0.87	1.23	1.16
	45 mins	585.95	0.73	3.8	3.73
	1 hr	526.17	0.66	4.45	4.38
	1.5 hrs	362.68	0.45	8.38	8.31
	2 hrs	335	0.42	8.82	8.75
	3 hrs	140.67	0.18	17.52	17.45
	4 hrs	108.08	0.14	20.95	20.88

Table 1 Continued.

21°C experiments				
static				
2 mins	608.62	0.76	2.04	1.97
5 mins	665.14	0.83	3.41	3.34
10 mins	617.08	0.77	6.41	6.34
10 mins	737.99	0.92	2.94	2.87
30 mins	359.9	0.45	7.66	7.59
45 mins	345.85	0.43	5.5	5.43
1 hr	493.34	0.62	1.44	1.37
1 hr	626.02	0.78	1.16	1.09
1 hr	426.92	0.53	1.95	1.88
1 hr	371.51	0.46	2.33	2.26
1 hr	490.08	0.61	1.84	1.77
1 hr	219.39	0.27	10.96	10.89
1.25 hrs	499.77	0.62	2.77	2.7
1.25 hrs	493.2	0.62	2.4	2.33
1.25 hrs	480.58	0.6	2.35	2.28
1.25 hrs	247.5	0.31	5.23	5.16
1.25 hrs	234.95	0.29	6.46	6.39
1.5 hrs	475.79	0.59	3.35	3.28
1.5 hrs	450.87	0.56	3.62	3.55
1.5 hrs	490.18	0.61	2.89	2.82
1.5 hrs	399.85	0.5	1.76	1.69
1.5 hrs	523.4	0.65	1.43	1.36
1.75 hrs	480.11	0.6	3.31	3.24
1.75 hrs	454.83	0.57	2.11	2.04
1.75 hrs	402.28	0.5	3.26	3.19
2 hrs	365.16	0.46	6.39	6.32
2 hrs	423.94	0.53	3.92	3.85
2 hrs	326.28	0.41	5.13	5.06
2.25 hrs	384.4	0.48	5.77	5.7
2.25 hrs	304.67	0.38	4.79	4.72
2.25 hrs	465.7	0.58	2.97	2.9

Table 1 Continued.

N$_2$ bubbling					
	5 mins	629.87	0.79	1.47	1.4
	10 mins	701.66	0.88	1.56	1.49
	20 mins	485.52	0.61	3.14	3.07
	30 mins	441.86	0.55	4.82	4.75
	45 mins	389	0.49	5.68	5.61
	1 hr	309.85	0.39	8.53	8.46
	1.25 hrs	185.24	0.23	12.38	12.31
50 °C experiments					
static					
	5 mins	574.74	0.72	2.2	2.13
	5 mins	609.33	0.76	1.95	1.88
	10 mins	641.57	0.8	1.72	1.65
	20 mins	564.36	0.71	1.8	1.73
	30 mins	293.41	0.37	6.1	6.03
	45 mins	128.31	0.16	16.53	16.46
	45 mins	247.38	0.31	3.98	3.91
	1 hr	171.5	0.21	5.97	5.9
N$_2$ bubbling					
	4 mins	652.64	0.82	1.4	1.33
	5 mins	471.82	0.59	3.46	3.39
	6 mins	448.01	0.56	4.11	4.04
	10 mins	405.78	0.51	5.18	5.11
	10 mins	339.87	0.42	6.15	6.08
	15 mins	395.23	0.49	4.75	4.68
	15 mins	351.65	0.44	5.77	5.7
	20 mins	225.44	0.28	8.66	8.59
	20 mins	251.14	0.31	7.62	7.55
	25 mins	181.02	0.23	9.9	9.83
	25 mins	134.8	0.17	10.75	10.68

Table 1 Continued.

70 °C experiments					
static					
	2 mins	528	0.66	3.59	3.52
	4 mins	337.44	0.42	5.23	5.16
	8 mins	322.28	0.4	2.8	2.73
	12 mins	333.26	0.42	3.51	3.44
	16 mins	157.29	0.2	9.01	8.94
	20 mins	123.31	0.15	9.57	9.5
N_2 bubbling					
	3 mins	431.38	0.54	3.61	3.54
	4 mins	328.69	0.41	4.87	4.8
	6 mins	263.21	0.33	5.77	5.7
	8 mins	273.99	0.34	5.08	5.01
	10 mins	224.74	0.28	6.1	6.03
	12 mins	90.29	0.11	12.11	12.04